

RSC Advances

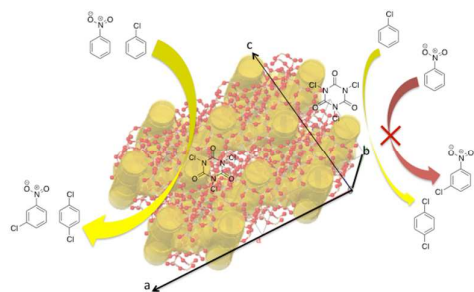


This is an *Accepted Manuscript*, which has been through the Royal Society of Chemistry peer review process and has been accepted for publication.

Accepted Manuscripts are published online shortly after acceptance, before technical editing, formatting and proof reading. Using this free service, authors can make their results available to the community, in citable form, before we publish the edited article. This *Accepted Manuscript* will be replaced by the edited, formatted and paginated article as soon as this is available.

You can find more information about *Accepted Manuscripts* in the [Information for Authors](#).

Please note that technical editing may introduce minor changes to the text and/or graphics, which may alter content. The journal's standard [Terms & Conditions](#) and the [Ethical guidelines](#) still apply. In no event shall the Royal Society of Chemistry be held responsible for any errors or omissions in this *Accepted Manuscript* or any consequences arising from the use of any information it contains.



Mass transfer limitations and catalytic activity were studied for various ZSM-5 zeolite crystal sizes in the chlorination of deactivated arenes. An estimation of the quantity of mild acidic external silanol groups of zeolite nanosheets was made.

MFI-type Zeolite Nanosheets for Gas-Phase Aromatics Chlorination:

A Strategy to Overcome Mass Transfer Limitations

Marilyne Boltz¹, Pit Losch¹, Benoit Louis^{1,*}, Guillaume Rioland², Lydie Tzanis²,

T. Jean Daou^{2,*}

¹ *Laboratoire de Synthèse Réactivité Organiques et Catalyse (LASYROC), UMR 7177, Institut de Chimie, Université de Strasbourg, 1 rue Blaise Pascal, 67000 Strasbourg Cedex.*

² *Université de Haute Alsace (UHA), CNRS, Équipe Matériaux à Porosité Contrôlée (MPC), Institut de Science des Matériaux de Mulhouse (IS2M) UMR 7361, ENSCMu, 68093*

Mulhouse Cedex, France.

Abstract

The continuous gas-solid (environmental-friendly) chlorination of deactivated arenes using trichloroisocyanuric acid (TCCA, C₃N₃O₃Cl₃) as chlorination agent was chosen to compare the catalytic performances of various MFI-type catalysts in a reaction demanding a strong acidity. Mass transfer limitations were also evaluated by reacting either chloro- or nitrobenzene through ZSM-5 zeolites porous network having different crystal sizes and morphologies. Whereas, the reaction rate was completely controlled by internal diffusion in 10-15 µm-sized big ZSM-5 zeolite crystals (Weisz modulus, $\phi_{\text{big crystals}} \sim 10$), the impact of internal diffusion could be ruled out for ZSM-5 nanocrystals (200-400 nm) and in stacked ZSM-5 nanosheets (thickness 2 nm). Based on reactivity differences in arenes halogenation between the two nano-sized ZSM-5 zeolites, we were able to estimate the quantity of mild acidic silanol groups in ZSM-5 nanosheets to roughly 1/3 of the total amount of Brønsted acid sites.

Keywords: chlorination, MFI zeolite, nanosheets, acid sites, Weisz modulus, nanocrystals

**Corresponding authors*

Email: jean.daou@uha.fr; blouis@unistra.fr

1. Introduction

Zeolites are crystalline materials possessing a well-defined porosity. These tectosilicates are obtained by the polymeric combination of TO_4 tetrahedra, where T can be either silicon or aluminum. The difference of valence between aluminum and silicon atoms induces the incorporation of a charge compensation cation within zeolite frameworks. If this cation is a proton, an intrinsic Brønsted acidity is present which, coupled with a high thermal stability, is responsible for zeolites interesting adsorption, diffusion and catalytic properties [1].

More than two hundred zeolite structures have been discovered during the past decades. However, only few of them have found an industrial application [2-6].

Zeolites are very important in petrochemical industry. Indeed, the acid sites present within the zeolite framework convert long saturated hydrocarbon molecules into smaller alkanes and alkenes, leading to fuel production [7]. However, the narrow pores of a zeolite may hinder the diffusion of big molecules [8]. The decrease in the catalytic performance and the generation of coke are two consequences of this diffusion issue. To solve that problem, both industry and academic researchers have struggled to develop new porous materials with enhanced catalytic properties [9]. Recently, several groups tempted to enhance the mass transfer in zeolite-catalyzed reactions, either via inhibiting the zeolite growth beyond the nanometer-scale to shorten diffusion paths [10-14], or by raising the zeolite pore size [15-17]. Another approach consists of introducing a hierarchical porosity, *i.e.*; *micro- and mesoporosities* (even macroporosity) within the zeolite crystals [18-23]. Despite a significant raise in the catalysts performance, these methods remain rather costly and sometimes hampered by stability issues, thus restricting their use at an industrial scale.

In 2009, Ryoo and co-workers christened the dawn of new zeolitic materials, by using specifically designed bifunctional compounds including at least two quaternary ammonium functions directing the formation of MFI zeolite, linked by an alkyl spacer and a hydrophobic alkyl chain inhibiting a further growth of the material [24,25]. They obtained well-defined nanosheets with a controllable thickness along crystallographic b-axis [26]. Recently, our

group showed that MFI-type zeolites with a lamellar morphology can be synthesized by using mononitrogen surfactants specifically designed by molecular modelling [27].

To date, only few investigations about the catalytic properties of MFI-type zeolite nanosheets have been carried out [28-33]. Kim *et al.* have shown that the product selectivity toward branched isomers could be continuously raised by diminishing the MFI zeolite crystal thickness to 2 nm [28]. They have also shown that MFI-type zeolite nanosheets exhibit longer catalytic lifetime and high selectivity for the production of ϵ -caprolactam via gas-phase Beckmann rearrangement of cyclohexanone oxime [29]. A linear correlation between the number of external strongest acid sites and the catalytic activity in decalin cracking could also be established [33].

In the present study, we report the influence of crystal morphology, *i.e.*; *nanosheets*, *nanocrystals*, *external surface-passivated nanocrystals* and *conventional coffin-shaped microcrystals* on the catalytic properties of MFI-type zeolites in a non-conventional gas-solid reaction that requires a strong acidity [34]. Our previous studies dealing with the chlorination of deactivated aromatics have shown the dependence between the catalytic activity and the acidity and pore topology of different zeolites [35,36]. Herein, we report the evaluation of the catalytic behaviour, *in the continuous nitrobenzene and chlorobenzene chlorinations with trichloroisocyanuric acid (TCCA)*, of four MFI-type zeolite samples exhibiting distinct crystal morphologies (nanocrystals, nanosheets, big crystals) or distinct surfaces (by external surface passivation).

2. Experimental

2.1 Structure directing agent synthesis

The di-quaternary ammonium-type surfactant, used for the MFI-type nanosheet synthesis, $[(C_{22}H_{45}-N^+(CH_3)_2-C_6H_{12}-N^+(CH_3)_2-C_6H_{13})Br_2]$ was obtained in two steps following the procedures reported by Choi *et al.* [24]. The surfactant was composed of a long-chain alkyl group (C_{22}) and two quaternary ammonium groups spaced by a C_6 alkyl linkage.

2.2 Zeolite syntheses

The MFI-type nanosheets were synthesized using the following procedures: 0.24 g of sodium hydroxide (Riedel de Haën, 99%) was dissolved in 7.17 g of distilled water in a 45 mL Teflon-lined stainless steel autoclave. 0.73 g of $C_{22}H_{45}-N^+(CH_3)_2-C_6H_{12}-N^+(CH_3)_2-C_6H_{13}Br_2$ and 0.07 g of aluminum sulfate (Rectapur) were then added, under stirring. After

homogenisation, 2.13 g of tetraethoxysilane (TEOS, Aldrich, 98%) were added, dropwise. Finally, 0.18 g of sulfuric acid (Aldrich) were added in order to set the molar composition of the gel to: 100 SiO₂ : 1 Al₂O₃ : 30 Na₂O : 18 H₂SO₄ : 10 C₂₂H₄₅-N⁺(CH₃)₂-C₆H₁₂-N⁺(CH₃)₂-C₆H₁₃Br₂ : 4000 H₂O. The gel was stirred at 1000 rpm during 30 min and placed in a tumbling oven at 150 °C for 4 days. The autoclaves were tumbled at 30 rpm. After synthesis, the product was filtered, washed with distilled water and dried overnight at 100 °C. The surfactants were finally removed by calcination in a muffle furnace at 550 °C for 8 h in air. The as-synthesized zeolite sample is denoted as ZSM-5 nanosheets.

For comparison, MFI-type zeolite nanocrystals were purchased from Zeolyst (CBV 5020) (denoted as ZSM-5 nanocrystals) and typical MFI zeolite large crystals with a coffin-shape morphology (denoted as big crystals) were synthesized in the same condition described above for MFI nanosheets. The only difference relied on 2.03 g of a tetrapropylammonium hydroxide (TPAOH) aqueous solution (20% in weight, Fluka) use instead of the appropriate amount of diquatery ammonium-type surfactant. The composition of the gel was therefore 100 SiO₂ : 1 Al₂O₃ : 30 Na₂O : 18 H₂SO₄ : 20 TPAOH : 4000 H₂O [27].

All the samples were NH₄⁺-ion-exchanged with a 1 M NH₄NO₃ aqueous solution at 65°C. The ion exchange process was repeated twice. After filtration and drying, NH₄⁺-ion-exchanged samples were calcined in air at 550 °C to obtain the zeolite H⁺-form.

The external surface acid sites of commercial nanosized zeolite (CBV 5020) were then passivated to obtain our fourth sample denoted as H-ZSM-5 nanocrystals-P. In a typical procedure, 1 g of H-ZSM-5 nanocrystals were suspended in a 4 wt.% TEOS solution (in 25 mL n-hexane) [37]. The suspension was heated for 1h under reflux. This procedure was repeated three-times to ascertain the complete passivation of external surface sites. Afterwards, the zeolite was filtered over a nylon membrane and the passivated H-form was obtained through calcination in an oven at 550 °C during 8 h in air.

2.3 Characterization of the zeolites

X-ray diffraction patterns of the different materials were recorded using a PANalytical MPD X'Pert Pro diffractometer operating with Cu K α radiation ($\lambda = 0.15418$ nm) equipped with an X'Celerator real-time multiple strip detector (active length = 2.122° 2 θ).

The size and the morphology of the crystals were determined by scanning electron microscopy (SEM) using a Philips XL 30 FEG microscope or a JEOL FEG 6700F microscope working at 9 kV accelerating voltage. Nitrogen adsorption / desorption isotherms were

measured using a Micromeritics ASAP 2420 apparatus. The specific surface area (S_{BET}) and microporous volume (V_{micro}) were calculated using BET and t -plot methods, respectively.

The Si/Al molar ratio of the zeolite was determined using the X-Ray Fluorescence (Philips, Magic X). H/D isotope exchange technique was used to determine the number of Brønsted acid sites present in the different solid acids [38-41].

2.4 Catalytic tests

All the catalytic tests were performed in an all-glass flow system with a cylindrical reactor. The gas flow (N_2) was regulated by means of Brooks 5850E mass flow controllers. The reactions were carried out by diluting the catalytic bed (TCCA and zeolite catalyst) in an amorphous matrix to maintain the same height for all catalytic beds. To investigate the influence of the MFI-type zeolite morphologies and crystal sizes on their catalytic performances, we have decided to work at iso-mass conditions. However, the catalyst weight was different for the two aromatics, being 62 mg and 250 mg for chlorobenzene and nitrobenzene, respectively.

Table 1 summarizes the reaction conditions used for either chlorobenzene or nitrobenzene chlorination reactions. The solid acid catalyst, the TCCA and the matrix were blended closely by grinding. The intimate solid mixture was then transferred to a cylindrical reactor and fixed to the set-up. The catalytic bed was first dried under dry nitrogen flow at 150 °C for 30 min. Then, the aromatic vapor pressure was allowed to pass through the catalyst bed for a defined reaction time.

The products were then trapped at – 196 °C and recovered downstream to the reactor with dichloromethane. The analysis was performed by gas chromatography (HP 6590) equipped with a capillary column (HP-5MS, 30 m). Retention times were compared with standards and used to characterize the different products. The degree of conversion and the selectivity toward the different products were calculated by taking into account the response factor of the substrate (aromatic) and those from the products (mono-, di- and trichlorinated aromatics) through the use of an external standard (styrene).

3. Results and discussion

3.1 Characterization

The crystallinity and purity of the three zeolite samples were checked by XRD. According to these patterns, the sole crystalline MFI phase was obtained for all zeolites

(Figure 1). As '*a priori*' expected, XRD reflections of ZSM-5 nanoparticles and ZSM-5 nanosheets are broader than those of micron-sized ZSM-5 big crystals synthesized in the presence of conventional structure directing agent (TPAOH). This can be explained by the smaller crystal size of ZSM-5 nanosheets and nanocrystals with respect to ZSM-5 crystals synthesized in the presence of TPAOH (Figure 2). In addition, for the ZSM-5 nanosheets, the major part of the diffraction lines belong to the (h0l) crystallographic plane, providing the sign that a one-dimensional growth-inhibition is undertaken along the *b*-axis, thus confirming the formation of nanosheets [25].

The SEM micrographs given in Figure 2 reveal the shape of the zeolite particles. ZSM-5 big crystals synthesized in the presence of TPAOH exhibit the characteristic prismatic shape of 10-15 μm in length. In contrast, MFI-type zeolite synthesized in the presence of diquatery ammonium surfactant exhibits a nanosheet morphology. A multi-lamellar stacking of MFI nanosheets was three-dimensionally intergrown. The overall thickness of the lamellar stacking was normally 20–40 nm. The zeolite layer was composed of three pentasil sheets, which corresponds to a single unit cell dimension along the *b*-axis (1.974 nm) [24]. The commercial MFI nanoparticles (ZSM-5 nanocrystals) exhibit spherical shape with an average size between 200 and 400 nm. As expected for microporous solids, typical type I nitrogen adsorption isotherms were observed for ZSM-5 nanocrystals and big crystals (Figure 3), with a slight hysteresis for ZSM-5 nanocrystals due to nanocrystals agglomeration. In the presence of the diquatery ammonium-type surfactant, the isotherms are of type I and IV. The presence of mesopores generated by the planar stacking of ZSM-5 nanosheets (intercrystalline porosity) is responsible for the higher adsorbed volume (mesoporous volume). The associated Brunauer-Emmett-Teller (BET) surface area, microporous volume and external surface of the three MFI-type zeolites are reported in Table 2.

3.2 Mass transfer evaluation and catalytic activity in the chlorination reactions

In this contribution, we have tested three different MFI zeolites in the continuous gas-solid phase chlorination of nitrobenzene and chlorobenzene to investigate the influence of crystal morphology. In parallel, ZSM-5 nanocrystals modified by silylation (named H-ZSM-5 nanocrystals P), adapted from Lercher *et al.* procedure [37], were also tested. Figures 4 and 5 present the nitrobenzene conversion and the selectivities toward monochlorination products and meta-chloronitrobenzene, and the chlorobenzene conversion, the selectivity to monochlorination products and the ortho / para ratio, respectively.

It is noteworthy that the selectivity in monochlorination products remain nearly the same for both nano-sized zeolites, being 60% toward meta-chloronitrobenzene produced as shown in Figure 4. Likewise, the selectivities toward o,p-dichlorobenzenes remained nearly equal for both zeolite nanocrystals and nanosheets (Figure 5).

Besides, one can observe that micron-sized ZSM-5 big crystals exhibit almost no activity (< 1 %) in both aromatics halogenation reactions. These results can be explained by a hindered diffusion in those large crystals with respect to the two nano-sized ZSM-5 zeolites.

In heterogeneous-catalyzed reactions by zeolites, especially involving bulky molecules, internal mass transfer limitations have to be taken into account [22,23,42].

The estimation of Thiele-Weisz modulus has therefore been undertaken according to the following formula: $\phi = RL^2 / (D_{\text{eff}} C_{\text{aromatic}})$ [42b], in which L represents the characteristic diffusion length, R the reaction rate, C_{aromatic} the substrate concentration and D_{eff} the effective diffusivity of a mono-substituted aromatic within the zeolite pores. A reaction rate of $5.2 \times 10^{-2} \text{ mol.m}^{-3}.\text{s}^{-1}$ was calculated for the more active sample and used for all estimations. Likewise, the same concentration of aromatic molecule as well as identical effective diffusion was used to determine Thiele-Weisz criteria, being 65.1 mol.m^{-3} and $10^{-14} \text{ m}^2.\text{s}^{-1}$, respectively. The characteristic diffusion length was defined by the crystal size [42b], thus the values were the followings: 30 nm (nanosheets), 300 nm (nanocrystals) and 15 μm (big crystals). A Thiele-Weisz modulus for micron-sized ZSM-5 big crystals $\phi_{\text{big crystals}} \sim 18$ was estimated, whereas $\phi_{\text{nanocrystals}} \sim 0.01$ and $\phi_{\text{nanosheets}} \sim 10^{-4}$ were obtained for ZSM-5 nanocrystals and nanosheets, respectively. In terms of intra-particle transport, the latter two values for Weisz modulus (admitted when $\phi < 0.1$) confirms a full utilization of zeolite catalyst particle, thus the reaction rate equals the intrinsic reaction rate [42,43]. In contrast, mass transfer issues completely hinder the reaction in micron-sized ZSM-5 big crystals ($\phi_{\text{big crystals}} \sim 18$). The superior catalytic performance of zeolite nanocrystals and nanosheets can therefore be rationalized by enhanced diffusion properties.

To further highlight the importance of diffusion phenomena, a comparison was drawn before and after the external surface passivation of ZSM-5 nanocrystals. It appeared that the silylated catalyst exhibited a lower activity for both aromatics, *i.e.*; 2% versus 19% for nitrobenzene (Figure 4), 7% versus 20% for chlorobenzene (Figure 5), respectively. The drastic loss in activity observed in aromatics chlorination reactions might be explained by both reduced microporous volume accessibility and decrease in BET surface area (*i.e.*; 321 m^2/g versus 402 m^2/g), which may impact nitrobenzene / chlorobenzene adsorption on the

acid sites within ZSM-5 channels. Hence, an influence of the acid site density was also evidenced while testing a nanocrystalline ZSM-5 (Zeolyst CBV 8020) having nearly 40% lower amount of Brønsted acid sites. Indeed, the rates of chlorobenzene converted referred to the amount of Al were 2.8×10^{-4} and 2.2×10^{-4} mol_{aromatic} converted / mol_{Al} / s for H-ZSM-5 nanocrystals (Si/Al=25) and Zeolyst CBV 8020 catalyst (Si/Al=40), respectively. A roughly 20% loss in the reaction rate was observed over MFI-type zeolite possessing roughly a 40% lower density of Brønsted acid sites. Besides the influence of ZSM-5 zeolite textural properties, it is worthy to mention here that the acid site density also influences, even moderately, the reactivity in the chlorination reaction.

Based on Weisz modulus estimations, internal mass transfer limitations could be excluded for all these nano-sized MFI zeolites. In spite of those Weisz moduli low values, one cannot neglect surface permeability barriers which are readily to occur in nanocrystals [44-46]. Krishna has highlighted discrepancies in the modelling of diffusion kinetics at high surface coverage by the reactants / products along with strong confinement effects [44]. Likewise, Karger *et al.* confirmed that these surface barriers may differ up to a factor 2, thus indicating a higher resistance for bulky molecules to enter inside the pores in smaller nanocrystals [45].

The difference between these two zeolites is related to their three-dimensional arrangement and to their textural properties. The ZSM-5 nanocrystals exhibit a specific surface area of 402 m²/g and a mesoporous volume of 0.08 cm³/g, whereas ZSM-5 nanosheets possess a specific surface area above 500 m²/g and a mesoporous volume of 0.48 cm³/g. In addition, ZSM-5 nanosheets exhibit a 30% higher number of Brønsted acid sites (1.17 versus 0.90 mmol H⁺/g for the ZSM-5 nanocrystals).

In the case of nitrobenzene chlorination (Figure 4), the two ZSM-5 catalysts led to nearly the same nitrobenzene conversion, *i.e.*; 19 % for the ZSM-5 nanocrystals and 18 % for the nanosheets. It is noteworthy that ZSM-5 nano-sized crystals / nanosheets improved significantly the catalytic performance of MFI-type catalysts when compared with conventional coffin-shaped big crystals. Unfortunately, the three-dimensional architecture of ZSM-5 nanosheets did not further raise the nitrobenzene reactivity in nano-sized ZSM-5 zeolites. Surprisingly, a 38% higher TOF was achieved over ZSM-5 nanocrystal catalyst, *i.e.*; 1.1×10^{-4} mol_{nitrobenzene} converted per acid site per m².g⁻¹ in one hour. The TOF values were corrected by the specific surface area values to avoid its influence.

In contrast, the two nano-sized MFI zeolites exhibited different activities in the chlorobenzene chlorination (Figure 5). Indeed, ZSM-5 nanosheets zeolite led to a twice higher

chlorobenzene conversion, with respect to the ZSM-5 nanocrystals, *i.e.*; 44 % versus 20 %. By taking into account TOF values, 1.9×10^{-3} and $2.8 \times 10^{-3} \text{ mol}_{\text{chlorobenzene conv.}} / \text{mol}_{\text{H}^+} / \text{m}^2 \cdot \text{g}^{-1} / \text{h}$ over ZSM-5 nanocrystals and nanosheets were reached, respectively. A nearly 33% higher TOF could therefore be achieved on ZSM-5 nanosheets, thus suggesting that the layer morphology in ZSM-5 nanosheets catalyst plays an important role in chlorobenzene chlorination. Ryoo and co-workers outlined the point that MFI nanosheets, thanks to their larger number of external acid sites, exhibited a higher catalytic activity for large organic molecules [24,25].

Nevertheless, the reverse tendency was observed for the nitrobenzene chlorination reaction which requires a stronger acidity due to the presence of deactivating *nitro-* group (TOF diminished by approx. 35%). Since the TOF values for the two nano-sized zeolites deviate from approx. $\pm 32\text{-}38\%$ ranging from chlorobenzene to nitrobenzene, one can roughly estimate the density of external silanol groups present at the nanosheets' outer surface, representing *thus nearly one third of the total amount of Brønsted acid sites*.

To summarize, ZSM-5 zeolite organization into nanosheet layers led to a 32% raise in the TOF for chlorobenzene halogenation, suggesting that all O-H groups from the catalyst are accessible and probably involved in the catalytic reaction whatever their localization and strength [35]. In contrast, the chlorination of nitrobenzene requires stronger Brønsted acid sites able to protonate TCCA molecule and thus to activate the chlorine atom [36]. One could therefore estimate the fraction of mild acidic external silanol groups in ZSM-5 nanosheets to roughly 1/3 of the total amount of Brønsted acid sites. Figure 6 summarizes the possible reaction of the aromatic substrate either within the zeolite porous network (for nitrobenzene and chlorobenzene) or at the external silanol groups from zeolite nanosheets (chlorobenzene only).

Mota *et al.* have developed a method to assess the acid strength of different solid acids with the use of linear free energy relationship for the H/D exchange with mono-substituted aromatics [47]. A combination of H/D exchange technique (to determine the whole number of O-H groups present in the zeolite) [41] with the present strategy to perform the halogenation reaction of various deactivated aromatics can therefore be used as a tool to estimate the fraction of acid sites involved in those electrophilic aromatic substitution reactions. Hence, one may distinguish the quantity of sites possessing milder acidity by tailoring the basicity of the probe molecule used for the reaction.

4. Conclusion

The gas-solid phase chlorination of deactivated arenes (chlorobenzene and nitrobenzene) using TCCA, was successfully performed over two nano-sized ZSM-5 zeolites. Whilst no change in the selectivity toward the reaction products could be evidenced, significant variations in TOF values were observed, *i.e.*; 1.9×10^{-3} and 2.8×10^{-3} $\text{mol}_{\text{conv. chlorobenzene}} / \text{mol}_{\text{H}^+} / \text{m}^2 \cdot \text{g}^{-1} / \text{h}$ over ZSM-5 nanocrystals and nanosheets, respectively. The reverse performance was observed for nitrobenzene, where a 38% higher TOF was achieved over ZSM-5 nanocrystals with respect to ZSM-5 nanosheets.

Acknowledgments

The authors are grateful to the Agence Nationale de la Recherche (ANR) for supporting the ANR-10-JCJC-0703 project (SelfAsZeo). PL would like to thank the National Research Fund Luxembourg for his PhD grant. The technical assistance from Thierry Romero and Jean-Daniel Sauer was highly appreciated.

References

- [1] M.E. Davis, *Nature* **417** (2002) 813.
- [2] C.H. Bartholomew, R.J. Farrauto, *Fundamentals of Industrial Catalytic Processes*, 2nd Ed., J. Wiley & Sons, New Jersey (2006) 60.
- [3] A. Corma, *Chem. Rev.* **95** (1995) 559.
- [4] J. Čejka, G. Centi, J. Perez-Pariente, W.J. Roth, *Catal. Today* **179** (2012) 2.
- [5] Z. Liu, Y. Wang, Z. Xie, *Chin. J. Catal.* **33** (2012) 22.
- [6] T.F. Degnan Jr, *Top. Catal.* **13** (2000) 349.
- [7] W. Vermeiren, J.P. Gilson, *Top. Catal.* **52** (2008) 1131.
- [8] D.M. Ruthven, M.F.M. Post, in : H. van Bekkum, E.M. Flanigen, P.A. Jacobs, J.C. Jansen (Eds.), *Introduction to Zeolite Science and Practice*, Elsevier, Amsterdam, 2001, 525.
- [9] A. Corma, *J. Catal.* **216** (2003) 298.
- [10] F.C. Buciuman, B. Kraushaar-Czarnetzki, *Catal. Today* **69** (2001) 337.
- [11] S. Mintova, N.H. Olson, V. Valtchev, T. Bein, *Science* **283** (1999) 958.
- [12] A. Zabala Ruiz, H. Li, G. Calzaferri, *Angew. Chem. Int. Ed.* **45** (2006) 5282.
- [13] F. Schüth, W. Schmidt, *Adv. Mater.* **14** (2002) 629.
- [14] L. Tosheva, V.P. Valtchev, *Chem. Mater.* **17** (2005) 2494.
- [15] D.M. Poojary, J.O. Perez, A. Clearfield, *J. Phys. Chem.* **96** (1992) 7709.

- [16] K.G. Strohmaier, D.E.W. Vaughan, *J. Am. Chem. Soc.* **125** (2003) 16035.
- [17] A. Corma, M.J. Diaz-Cabanas, J.L. Jorda, C. Martinez, M. Moliner, *Nature* **443** (2006) 842.
- [18] K. Egeblad, C.H. Christensen, M. Kustova, C.H. Christensen, *Chem. Mater.* **20** (2008) 946.
- [19] R. Chal, C. Gerardin, M. Bulut, S. van Donk, *ChemCatChem* **3** (2011) 67.
- [20] R. Garcia, I. Diaz, C. Marquez-Alvarez, J. Perez-Pariente, *Chem. Mater.* **18** (2006) 2283.
- [21] B. Louis, G. Laugel, P. Pale, M.M. Pereira, *ChemCatChem* **3** (2011) 1263.
- [22] B. Louis, F. Ocampo, H.S. Yun, J.P. Tessonnier, M.M. Pereira, *Chem. Eng. J.* **161** (2010) 397.
- [23] J. Perez-Ramirez, C.H. Christensen, K. Egeblad, C.H. Christensen, J.C. Groen, *Chem. Soc. Rev.* **37** (2008) 2530.
- [24] M. Choi, K. Na, J. Kim, Y. Sakamoto, O. Terasaki, R. Ryoo, *Nature* **461** (2009) 246.
- [25] K. Na, M. Choi, W. Park, Y. Sakamoto, O. Terasaki, R. Ryoo, *J. Am. Chem. Soc.* **132** (2010) 4169.
- [26] W. Park, D. Yu, K. Na, K.E. Jelfs, B. Slater, Y. Sakamoto, R. Ryoo, *Chem. Mater.* **23** (2011) 5131.
- [27] J. Dhainaut, T.J. Daou, Y. Bidal, N. Bats, B. Harbuzaru, G. Lapisardi, H. Chaumeil, A. Defoin, L. Rouleau, J. Patarin, *CrystEngComm* **15** (2013) 3009.
- [28] J. Kim, W. Kim, Y. Seo, J-C. Kim, R. Ryoo, *J.Catal.* **301** (2013) 187.
- [29] J. Kim, W. Park, R.Ryoo, *ACS Catal.* **1** (2011) 337.
- [30] E. Verheyen, C. Jo, M. Kurttepel, G. Vanbutsele, E. Gobechiya, T.I. Korányi, S. Bals, G. van Tendeloo, R.Ryoo, C.E.A. Kirschhock, J.A. Martens, *J.Catal.* **300** (2013) 70.
- [31] S. Hu, J. Shan, Q. Zhang, Y. Wang, Y. Liu, Y. Gong, Z. Wu, T. Dou, *App. Catal. A* **445-446** (2012) 215.
- [32] K. Na, C. Jo, J. Kim, W-S. Ahn, R. Ryoo, *ACS Catal.* **1** (2011) 901.
- [33] Y. Seo, K. Cho, Y. Jung, R. Ryoo, *ACS Catal.* **3** (2013) 713.
- [34] T.J. Daou, M. Boltz, L. Tzanis, L. Michelin, B. Louis, *Catal. Commun.* **39** (2013) 10.
- [35] G.F. Mendonça, A.R. Bastos, M. Boltz, B. Louis, P. Pale, P.M. Esteves, M.C.S. de Mattos, *Appl. Catal. A* **460-461** (2013) 46.
- [36] M. Boltz, M.C.S. de Mattos, P.M. Esteves, P. Pale, B. Louis, *Appl. Catal. A* **449** (2012) 1.
- [37] S. Zheng, H. R. Heydenrych, H. P. Röger, A. Jentys, J. A. Lercher, *Top. Catal.* **22** (2003) 101.
- [38] B. Louis, S. Walspurger, J. Sommer, *Catal. Lett.* **93** (2004) 81.
- [39] J.P. Tessonnier, B. Louis, S. Walspurger, J. Sommer, M.J. Ledoux, C. Pham-Huu, *J. Phys. Chem. B.* **110** (2006) 10390.
- [40] S. Walspurger, B. Louis, *Appl. Catal. A* **336** (2008) 109.
- [41] B. Louis, A. Vicente, C. Fernandez, V. Valtchev, *J. Phys. Chem. C* **115** (2011) 18603.
- [42] a) M. Baerns, H. Hofmann, A. Renken, *Chemische Reaktionstechnik*, 3rd ed., Georg Thieme Verlag, Stuttgart, Germany, 1999. b) B. Louis, L. Kiwi-Minsker, P. Reuse, A. Renken, *Ind. Eng. Chem. Res.* **40** (2001) 1454.

- [43] O. Levenspiel, *Chemical Reaction Engineering*, 3rd ed., John Wiley & Sons, New York, United States, 1999.
- [44] R. Baur, R. Krishna, *Catal. Today* **105** (2005) 173.
- [45] D. Tzoulaki, L. Heinke, H. Lim, J. Li, D. Olson, J. Caro, R. Krishna, C. Chmelik, J. Karger, *Angew. Chem. Int. Ed.* **48** (2009) 3525.
- [46] L. Karwacki, M.H.F. Kox, D.A.M. de Winter, M.R. Drury, J.D. Meeldijk, E. Stavitski, W. Schmidt, M. Mertens, P. Cubillas, N. John, A. Chan, N. Kahn, S.R. Bare, M. Anderson, J. Kornatowski, B.M. Weckhuysen, *Nat. Mater.* **8** (2009) 959.
- [47] V.L.C. Gonçalves, R.C. Rodrigues, R. Lorençato, C.J.A. Mota, *J. Catal.* **248** (2007) 158.
- [48] E.L. First, C.E. Gounaris, J. Wei, C.A. Floudas, *Phys. Chem. Chem. Phys.* **13** (2011) 17339.

Table captions

Table 1. Experimental conditions for aromatics chlorination reaction.

Table 2. Textural properties of the zeolites measured by N₂ sorption.

Table 3. Chemical composition (Si/Al molar ratio) and Brønsted acidity of four MFI-type zeolites.

Aromatic	TCCA equivalent (mol)	Aromatic equivalent (mol)	Acid Site equivalent (mol)	Diluting agent	T _{reaction} (°C)	T _{aromatic trap} (°C)	Flow rate (mL/min)	Reaction duration (h)
Nitrobenzene	2.5.10 ⁻⁴	2.5.10 ⁻⁴	2.5.10 ⁻⁴	silica	150	r.t.	100	5
Chlorobenzene	5.0.10 ⁻⁴	5.0.10 ⁻⁴	1.0.10 ⁻⁴	glass rings	150	0	25	3

Table 1

Zeolite	S _{BET} (m ² /g)	V _{micro} (cm ³ /g)	V _{meso} (cm ³ /g)
H-ZSM-5 nanosheets	503	0.18	0.48
H-ZSM-5 big crystals	351	0.18	0
H-ZSM-5 nanocrystals	402	0.18	0.08
H-ZSM-5 nanocrystals P	321	0.18	0.07

Table 2

Zeolite	Si / Al	Brønsted acid sites [mmol/g]
H-ZSM-5 nanosheets	48	1.17
H-ZSM-5 big crystals	28	0.59
H-ZSM-5 nanocrystals	25	0.90
H-ZSM-5 nanocrystals P	49	0.37

Table 3

Figure captions

Figure 1. XRD patterns of ZSM-5 zeolites, big crystals (a), nanocrystals (b), nanosheets (c).

Figure 2. SEM micrographs of ZSM-5 zeolites, big crystals (a), nanosheets (b), nanocrystals (c).

Figure 3. N₂ adsorption-desorption isotherms of ZSM-5 zeolites, big crystals (solid circles), nanosheets (empty circles), nanocrystals (empty square).

Figure 4. Nitrobenzene chlorination reaction over the four MFI-type zeolite samples

Figure 5. Chlorobenzene chlorination reaction over the four MFI-type zeolite samples

Figure 6. Schematic representation of aromatics reaction over ZSM-5 nanosheets: either within the pore network or at the external surface. The zeolite model has been taken from ref. [48].

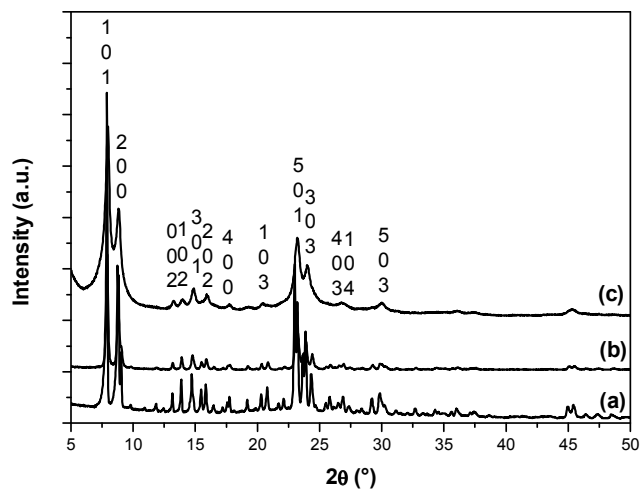


Figure 1

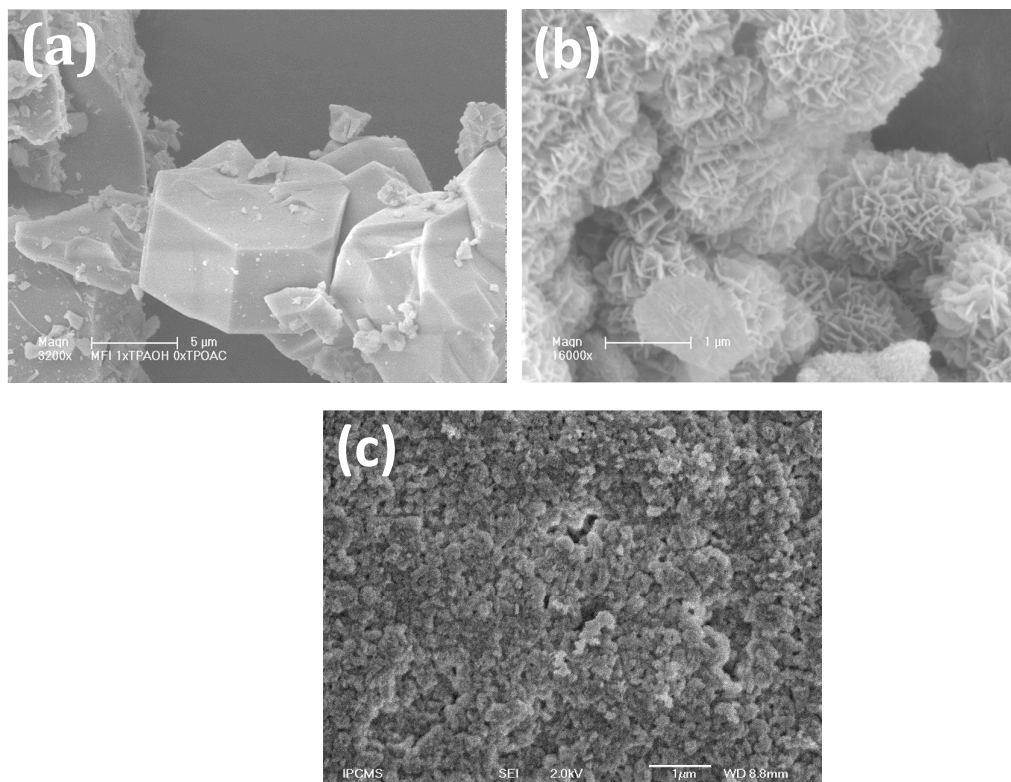


Figure 2

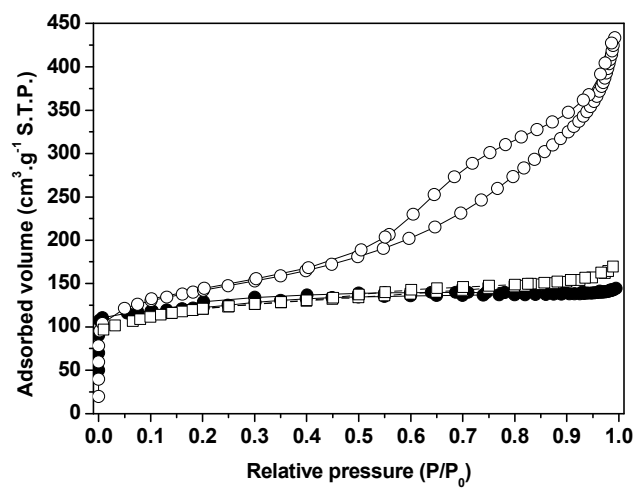


Figure 3

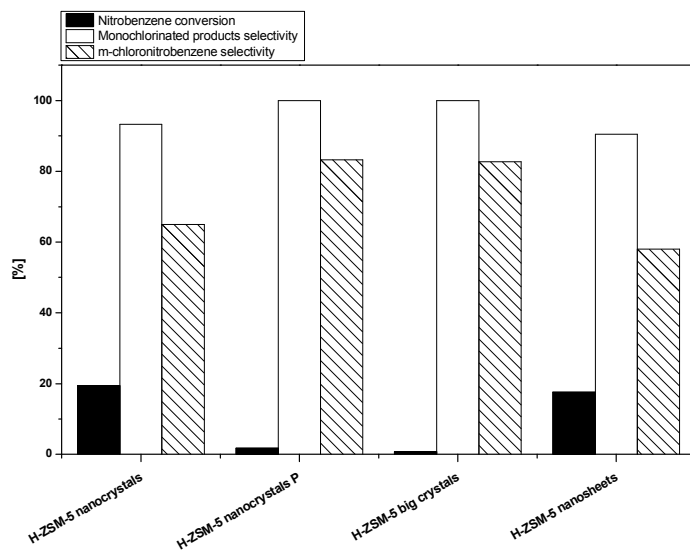


Figure 4

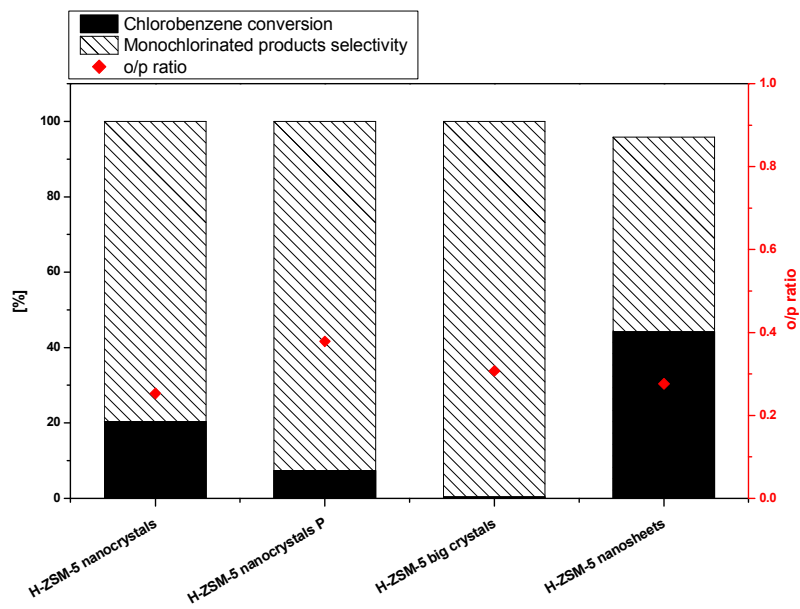


Figure 5

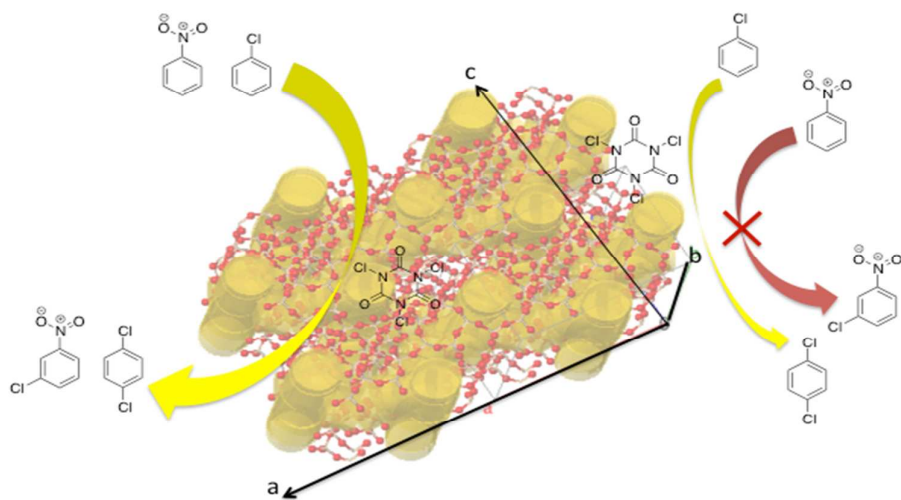


Figure 6